DR. RICARDO GERMAN DUNGER (Orcid ID : 0000-0001-7307-6792)

Article type : Original Article

Running title: ADV affects plant physiology

Running author: C. Jaime et al.

Morphological changes, alteration of photosynthetic parameters and chlorophyll production induced by infection with alfalfa dwarf virus in *Medicago sativa* plants

C. Jaime[ab], S. E. Muchut[cd], A.G. Reutemann[cd], J. Gieco[a] and G. Dunger[ad]*

[a]*Universidad Nacional del Litoral, Facultad de Ciencias Agrarias, Departamento de Producción Animal, Esperanza, Santa Fe;* [b]*Universidad Nacional del Litoral; Facultad de Bioquímica y Ciencias Biológicas, Santa Fe;* [c]*Universidad Nacional del Litoral, Facultad de Ciencias Agrarias, Departamento de Biología Vegetal, Esperanza, Santa Fe; and* [d]*Consejo Nacional de Investigaciones Científicas y Técnicas (CONICET), Argentina*

*E-mail: gdunger@fca.unl.edu.ar

In Argentina, infections by alfalfa dwarf virus (ADV) affect the cultivation of alfalfa, which is globally one of the most important forage plants. The main objective of this study was to improve current understanding of the underlying mechanisms related to the dwarfism phenotype developed during viral infection. Hydrogen peroxide production, callose deposition and *PR5* gene expression levels were evaluated to determine if ADV induces plant defence responses. At the morphological level, higher epicuticular wax production and an increase in proliferation of cells from the fundamental parenchyma were observed when plants were infected by ADV. Infected plants had reduced photosynthesis, stomatal conductance and transpiration/evaporation rate, but interestingly

This article has been accepted for publication and undergone full peer review but has not been through the copyediting, typesetting, pagination and proofreading process, which may lead to differences between this version and the Version of Record. Please cite this article as doi: 10.1111/PPA.13109

the production of chlorophylls was induced. Finally, using transcriptional analysis, ADV was observed to negatively affect the expression of genes related to synthesis of auxins, cytokinins and brassinosteroids. These results suggest that ADV infection induces a hormonal imbalance leading to an increase in chlorophyll pigment synthesis, stomatal closure and generation of tissue deformation. Overall, the results show a morphological, physiological and photosynthetic characterization of dwarf plants affected by ADV.

Keywords: chlorophyll, dwarfism, forage, phytohormones

Introduction

Alfalfa (*Medicago sativa*) is a perennial plant with high nutritional value, rich in minerals (calcium, phosphorus, potassium, magnesium and sulphur) and vitamins (Radović *et al.*, 2009). The global production of alfalfa is distributed across an area exceeding 35 million ha over more than 80 countries (Radović *et al.*, 2009).

Due to its forage quality, the global demand for alfalfa has increased, mainly for use as dairy cattle feed, and for the production of feed for other animals. Alfalfa is one of the world's most versatile crops. Although its optimal growth temperature is around 24 °C, it grows both in subtropical conditions and in temperate environments. Alfalfa can also grow on soils ranging from sandy to clay.

The quality of the crop is compromised by the attack of pests and by several diseases caused by diverse viruses, fungi and bacteria (Samac *et al.*, 2014). An important disease is dwarfism, which is caused by infection with different viruses, among them the alfalfa dwarf virus (ADV). *Alfalfa dwarf virus* belongs to the family *Rhabdoviridae* and has been grouped in the genus *Cytorhabdovirus*. It has a non-segmented, negative-sense, single-stranded RNA genome of 14491 nucleotides (Bejerman *et al.*, 2015; Whitfield *et al.*, 2018). The genome encodes 7 proteins: nucleocapsid protein (N), phosphoprotein (P), movement protein (P3), matrix protein (M), glycoprotein (G), unknown protein (P6) and RNA-dependent RNA polymerase (L) (Bejerman *et al.*, 2015).

Alfalfa plants infected with dwarf virus show shortened internodes, leaf puckering and varying-sized vein enations (hyperplastic outgrowths) on the abaxial leaf surface (Bejerman *et al.*, 2011). The exact mechanism of viral transmission is not clear, but some authors point to the aphid *Aphis craccivora* as the vector (Samarfard *et al.*, 2018). Although specific mechanisms by which cytorhabdoviruses infect plants have been reported (Mann *et al.*, 2016), more efforts are needed to understand the infection process. In order to study the role of the main phytohormones responsible for the morphological deformities and dwarfism, transcriptional expression analysis was carried out for the genes encoding YUCCA flavin monooxygenase 6 (*YUC6*; Cheng *et al.*, 2007) and isopentenyl transferase (*IPT*; Argueso *et al.*, 2009) involved in the biogenesis of auxins and cytokinins (CKs) respectively, and brassinosteroid-6-oxidase 2 (*BR6OX2*; Shimada *et al.*, 2003) and steroid 22-alpha-hydroxylase (*DWF4*; Sakamoto *et al.*, 2006) involved in the biogenesis of brassinosteroids (BRs). This study performed a general characterization at the molecular, biochemical, histological, micromorphological and photosynthetic level of the effect of ADV on alfalfa plants to determine the extent and location of damage caused by the infection. Additionally, it showed that ADV induces drastic morphological changes, production of chlorophyll pigments, stomatal closure and epicuticular wax accumulation. The results shown here have important implications regarding plant–pathogen interactions involving one of the most important forage crops in the world.

Materials and methods

Plant materials

Alfalfa plants were grown in a greenhouse at 25 °C with a 16:8 h light:dark photoperiod. ADV was isolated from alfalfa plants collected from fields in Esperanza district, Santa Fe, Argentina. The presence of ADV and the absence of alfalfa enamovirus-1 (AEV-1), alfalfa mosaic virus (AMV), alfalfa latent virus (ALV) and alfalfa leaf curl virus (ALCV) in the sap of infected plants was confirmed by PCR assays. To analyse the presence/absence of ADV, AEV-1, AMV and ALV, total RNA was extracted by homogenizing alfalfa leaves in 0.1 M potassium phosphate buffer (pH 7.0) in a liquid nitrogen-cooled mortar and pestle. RNA was isolated using 1 mL TRIzol reagent (Thermo Fisher Scientific) and was then subjected to reverse transcription using the Revert Aid H Minus First Strand cDNA Synthesis kit (Thermo Fisher Scientific) according to the

manufacturer's instructions and as described in detail below. To analyse the presence/absence of ALCV, total DNA was extracted using the cetyltrimethylammonium bromide (CTAB) method and precipitated with isopropanol. PCR assays were performed using cDNA or genomic DNA as template and the specific primers listed in Table S1. Mechanical inoculation was performed by gently rubbing silicon carbide powder (400 mesh; Sigma-Aldrich) and sap from ADV-infected alfalfa leaves in 0.1 M potassium phosphate buffer (pH 7.0) onto the surface of 5−10 upper leaflets of 1-month-old plants, using a latex-gloved finger. The negative control was performed by mock inoculating leaflets with buffer (0.1 M potassium phosphate buffer, pH 7.0). The leaves were washed with running tap water for 10 s following inoculation. Sap was prepared by homogenizing infected leaves in 0.1 M potassium phosphate buffer (pH 7.0) using a liquid nitrogen-cooled mortar and pestle. Plants were grown for 4–10 months in individual 5 L pots with soil and perlite (2:1 v/v) and covered with an anti-aphid net in a greenhouse. PCR assays using the primers listed in Table S1 were carried out to confirm the ADV infection.

Scanning electron microscopy (SEM)

For each treatment, one leaf was collected from each of five plants, 7 months after inoculation with ADV or buffer. The leaf fragments were fixed in formaldehyde:ethanol:acetic acid:water (FAA; 10:50:5:35 v/v/v/v) for 24 h and then transferred to 70% (v/v) ethanol. Samples were dehydrated under increasing concentrations of ethanol (70%, 80%, 96%, 100% v/v), washed twice with 100% acetone, and dried by critic point (Emitech K850) using CO_2 as intermediate fluid. The dried materials were coated with gold–palladium using a Sputter Coater system (Emitech SC7640) and then visualized in a QUANTA 200 (FEI, Thermo Fisher Scientific) scanning electron microscope.

Histological observation

Histological study was performed as described by Gonzalez & Marazzi (2018) with modifications. For each treatment, one leaf was randomly collected from each of five plants, 7 months after inoculation with ADV or buffer. The leaf material was fixed for 48 h in FAA and preserved in 70% (v/v) ethanol. Leaves were sectioned in pieces containing the enation protruding from the abaxial zone, and were then dehydrated through a gradual ethanol series (80%, 90%, 96%, 100%

v/v). Samples were clarified using ethanol–xylene at increasing concentrations of xylene, and embedded in paraffin. Transversal serial sections from the paraffin blocks including the sample were cut with a rotary microtome (Leica RM2125 RTS) at 18 µm and stained with safranin (Sigma-Aldrich) and astra blue (Biopack). Samples were mounted on glass slides with Canada balsam, observed under a light microscope (Leica DM1000), and photographed using a digital camera (EOS REBEL T2i; Canon). Images were analysed and processed using IMAGEJ (https://fiji.sc/).

Hydrogen peroxide detection

Hydrogen peroxide production in alfalfa plants was detected using 3,3-diaminobencidine (DAB; Sigma Aldrich) as described previously (Dunger *et al.*, 2005). For each treatment, a total of five leaves were excised from three plants, 5 months after inoculation with ADV or buffer, and incubated with 1 mg mL^{-1} DAB solution for 18 h in the dark. Then leaves were immersed in ethanol 96% (v/v) and incubated at 37 °C until complete discoloration. Five fragments from each leaf were mounted and visualized by fluorescence microscopy (Leica M205 FAC) using magnifications of ×40 and ×60. Grey-scale images obtained were analysed and processed as previously described by Hatsugai *et al.* (2016) using IMAGEJ. The stained areas were identified by using the threshold feature and processed using the vector H DAB from the colour deconvolution plug-in. Parameter settings were kept constant throughout all analyses.

Observation of callose deposition

For each treatment, five leaves were randomly collected from each of three alfalfa plants, 5 months after inoculation with ADV or buffer, and fixed in a 1:1 (v/v) acetic acid:ethanol solution for 18 h and then cleared in 96% (v/v) ethanol. Then leaves were washed twice in phosphate buffer (0.07 M, pH 9.0) and finally incubated for 5 h in 0.1% (w/v) aniline blue (Sigma Aldrich). Five fragments from each leaf were washed with phosphate buffer (0.07 M, pH 9.0), mounted on slides and visualized on a fluorescence microscope (Leica M205 FAC) using ×10, ×40 and ×60 magnifications. Images were analysed and processed as previously described by Zavaliev & Epel (2015) using IMAGEJ. Images were converted to 8-bit TIF format and pixel thresholds were set for

each image using the threshold tool. The rolling ball radius was set at 30.0 pixels during the process of subtracting background. The auto local threshold was adjusted using the Bernsen method and a radius of 10.0 pixels. The analysis was made using particles from 3 to 100 pixel^2 and a circularity of 0.5 to 1.0 pixel. Parameter settings were kept constant throughout all analyses.

Wax quantification

Epicuticular wax extraction was performed as described by Bewick *et al.* (1993) with modifications. For each treatment, two leaves (second pair of leaves below the apical bud) were collected from each of five plants, 5 months after inoculation with ADV or buffer. Plant material was washed with water, air dried and dipped in 50 mL chloroform for 20 s. Then, the leaves were fixed fully expanded on a paper sheet to quantify the total leaf area using a scanner (HP Deskjet 2050) and IMAGEJ. The solution (chloroform and wax) was transferred to a preweighed flask. After complete chloroform evaporation under vacuum, the flask was weighed to obtain the content of epicuticular wax per leaf area.

Quantification of chlorophyll pigments and photosynthetic parameters

Chlorophyll *a* and *b* were extracted with acetone and quantified spectrophotometrically. For each treatment, 2 g leaf material was collected from the second leaf below the apical bud of five plants, 5 months after inoculation with ADV or buffer. Leaf material was homogenized using liquid nitrogen and incubated at 4 °C in 90% (v/v) acetone for 18 h in the dark. Then, samples were centrifuged at 1000 ***g*** for 5 min. Absorbance was measured at 646, 663 and 750 nm using a UV-VIS spectrophotometer (Hitachi U2000). Estimation of chlorophyll *a* and *b* was performed by using the extinction coefficients and equations previously determined by Wellburn (1994).

For each treatment, two mature fully-expanded leaves were selected from each of five plants (second pair of leaves below the apical bud), 5 months after inoculation with ADV or buffer. The leaf material was used to determine net photosynthesis (Pn), stomatal conductance (GS) and transpiration/evaporation rate (E). The measurements were made using a portable

photosynthesis system (CIRAS-2; PP System). The concentration of CO_2 was set at 500 ppm and photon flux density at 900 μmol m^{-2} s^{-1} and maintained constant during the experiments.

RNA extraction and quantitative RT-PCR

For each treatment, root, stem and leaf samples were collected from three 6-month-old alfalfa plants, 5 months after inoculation with ADV or buffer. The samples were washed with sterilized water and then homogenized using a liquid nitrogen-cooled mortar and pestle. Total RNA from 100 mg of vegetative tissue was isolated using 1 mL TRIzol reagent (Thermo Fisher Scientific) according to the manufacturer's instructions. Briefly, samples with TRIzol were incubated for 10 min at 65 °C before mixing with chloroform (0.2 mL per mL TRIzol). Samples were centrifuged at 12 000 ***g*** for 15 min at 4 °C, the upper aqueous phase was collected, and the RNA was precipitated with isopropanol. After the extraction was completed, RNA was resuspended in 20 μL RNase-free distilled H_2O (Thermo Fisher Scientific) and the RNA was quantified spectrophotometrically. The RNA extracts were treated with RNase-free DNase I (Thermo Fisher Scientific) to avoid DNA contamination. The RNA (1 μg) was subjected to reverse transcription using the Revert Aid H Minus First Strand cDNA Synthesis kit (Thermo Fisher Scientific) following the manufacturer's instructions and using 100 pmol of random hexamer primers (10 min at 25 °C, 30 min at 50 °C and 5 min at 85 °C). Quantitative real-time PCR was performed using an AriaMx Real Time PCR System (Agilent Technologies). Reactions were performed with Maxima SYBR Green/ROX qPCR Master Mix (Thermo Fisher Scientific), 200 ng cDNA as template and specific oligonucleotides (0.3 μM) for amplification of the genes coding for the pathogenesis-related (PR) protein 5 (PR5), brassinosteroid-6-oxidase 2 (BR6OX2), steroid 22-alpha-hydroxylase (DWF4), YUCCA flavin monooxygenase 6 (YUCCA6), isopentenyl transferase (IPT), magnesium-chelatase subunit chlH (CHLH), magnesium-protoporphyrin IX methyltransferase (CHLM), hydroxymethylbilane synthase (HEMC), 18S ribosomal RNA and actin2 (for primer sequences see Table S1). Oligonucleotides for candidate and normalizer genes were designed using Primer3 software. Quantitative analysis was performed using the following protocol: an initial denaturation step of 10 min at 95 °C, followed by 40 cycles of 30 s at 95 °C and 30 s at 60 °C. To ensure that the reaction was quantitative, amplification efficiencies were calculated from serial dilutions of the cDNA template, and only primer pairs with efficiencies

>90% ($R^2 > 0.99$) were used. Expression of the candidate genes was normalized against that of the 18S ribosomal RNA and *actin2* genes as an internal reference. To determine quantitatively the transcript levels of genes, the $2^{-\Delta\Delta Ct}$ method was used as described by Livak & Schmittgen (2001) and with three technical replicates for each biological replicate. PCR assays, using the specific primers listed in Table S1, were performed to confirm the ADV infection in the alfalfa plants used in this study.

Counting of stomata

Quantification of stomata was performed by observation of negative images as described by Gudesblat *et al.* (2007), with modifications. For each treatment, five fully expanded alfalfa leaves were randomly collected from each of five plants (second leaf below the apical bud, 25 leaves per treatment), 5 months after inoculation with ADV or buffer. The leaflets were fixed to a glass slide using a clear double-sided adhesive tape (3M). The mesophyll was removed using a 1:1 (v/v) solution of sodium hypochlorite and scraped with a scalpel blade keeping the abaxial epidermis attached to the tape. Samples were immediately washed with water and observed in a microscope (Leica M205 FAC).

Statistical analysis

Data from experiments were analysed using the SigmaPlot (Systat) software by two-sample Student's *t*-test. A *P*-value of less than 0.05 (*), 0.01 (**) or 0.001 (***) was considered to indicate a statistically significant difference. Data from the experiments were expressed as mean ± SE.

Results

Morphological characterization

As previously reported by Bejerman *et al.* (2011), abnormal leaf morphology was observed in a high proportion of infected plants, characterized by curling of the leaves and formation of enations

on the abaxial zone, especially in the rib and midrib zones (Fig. 1a–d). These prominent enations were clearly visible in infected plants and could reach 3–4 mm (Fig. 1c,d). The SEM analysis revealed that the epidermal tissue of abaxial surfaces of ADV-infected leaves presented normal cell morphology, even in the enations developed in the ribs (Figs 2 & S1). However, into the mesophyll, a disorganized growth pattern of the fundamental parenchyma cells belonging to the ribs of infected plants was found (Fig. 3a–c). This condition was observed both in small (Fig. 3a) and main (Fig. 3b,c) vascular bundles. These observations suggest that the enation development is potentially a consequence of an uncontrolled parenchyma cell proliferation induced by the infection.

Plant defence responses to ADV infection

To determine if alfalfa plants deploy defence mechanisms against infection by ADV, the production of reactive oxygen species (ROS) hydrogen peroxide (H_2O_2), the callose deposition and the transcript expression of the pathogenesis-related gene *PR5* were analysed. The substrate DAB polymerizes in contact with H_2O_2, producing a reddish-brown precipitate (Dunger *et al.*, 2005). When ADV-infected alfalfa leaves were stained with DAB, a significantly higher long-term accumulation of H_2O_2 was observed on the vascular system compared to control plants ($t = 2.3$, df = 8, $P = 0.00001$; Fig. 4a,b,e). Also, when callose deposition was evaluated, ADV-infected alfalfa leaves showed a higher number of fluorescent callose spots compared to the control plants ($t = 4.3$, df = 8, $P = 0.02$; Fig. 4c,d,f). Additionally, when the transcript level of *PR5* was analysed, a slightly higher expression ($P > 0.05$) in leaves of ADV-infected plants was observed (Fig. 4g).

Observation and quantification of epicuticular wax

Through SEM analysis, accumulation of epicuticular wax was found in leaves of ADV-infected plants (Fig. 5a,b). To confirm this observation, the alfalfa epicuticular wax was extracted using chloroform, and a significantly ($t = 2.3$, df = 7, $P = 0.0001$) higher wax proportion was found on infected leaves compared to the control (Fig. 5c).

Evaluation of photosynthetic parameters and pigment production

In order to evaluate the effect of the infection by ADV on photosynthesis, the net photosynthesis (Pn), the stomatal conductance (Gs) and the transpiration/evaporation rate (E) were analysed (Fig. 6). Infection by ADV significantly affected the net photosynthetic parameters by decreasing the photosynthesis rate by 40% compared to control plants (t = 2.8, df = 4, P = 0.0008; Fig. 6a). Similar values were found for the stomatal conductance (t =2.6, df = 5, P = 0.002; Fig. 6b) and the transpiration/evaporation rate (t = 2.8, df = 5, P = 0.009; Fig. 6c). Strikingly, ADV-infected leaves showed a darker green colour in relation to the control plants (Fig. 1a). In order to understand this observation, the photosynthetic pigments chlorophyll *a* (Chl *a*) and *b* (Chl *b*) were quantified. A slightly increased content of Chl *a* and Chl *b* was found in treated alfalfa (Table 1) but the Chl *a*:Chl *b* ratio (2.541 in ADV-infected plants) was not significantly different (P > 0.05) from that observed in control plants (2.761) (Table 1). Seeking an explanation to the altered photosynthetic parameters observed during the viral infection, a microscopic analysis was performed to determine the total number of opened and closed stomata per mm^2 (Fig. 7). On average (P > 0.05, n = 16), a total of 81 stomata per mm^2 were observed on the abaxial side of infected leaves versus 125 stomata per mm^2 on the control leaves (Fig. 7a). In infected leaves, 43.2% of stomata remained open; in contrast, when control leaves were analysed, 74.4% of stomata were open (Fig. 7a). In order to understand the reason for the high levels of chlorophyll pigments during ADV infection, the transcript levels of genes involved in chlorophyll biosynthesis were determined (Fig. 7b). The expression of *HEMC, CHLH* and *CHLM* genes was induced 3.5-fold (*HEMC*), 2.1-fold (*CHLH*) and 3.0-fold (*CHLM*) in infected alfalfa plants (Fig. 7b). This result suggests that the biosynthesis of these pigments could be induced during the infection process.

Transcriptional analysis of hormone-related genes

Transcript analysis of genes involved in the biosynthesis of auxins, CKs and BRs was undertaken to study the physiological mechanisms involved in the induction of dwarfism during the viral infection (Fig. 7c). The expression of the genes that participate in the biosynthesis of BRs (*BR6OX2*), auxins (*YUC6*) and CKs (*IPT*) were reduced in plants infected with ADV. In contrast, the expression of the *DWF4* gene was up-regulated during viral infection (Fig. 7c).

Discussion

The infection by ADV reduces the yield of alfalfa hay, generating significant economic losses and making meat and milk production more expensive (Lenardon *et al.*, 2010). Alfalfa plants severely affected by ADV have a characteristic dwarfism phenotype that significantly reduces the biomass production (Bejerman *et al.*, 2011). The induction of dwarfism in plants is due to a combination of molecular and physiological factors (Bejerman *et al.*, 2015; Jin *et al.*, 2016). In some cases, severe dwarfism has been observed as result of a multiple virus infection (Bejerman *et al.*, 2016). This report addressed this issue at molecular levels, and aimed to understand the mechanisms implicated in the generation of morphological changes during the viral infection. The study showed that ADV is involved in important processes both at physiological and transcriptional levels.

Plant virus infection often includes symptoms such as morphological changes, leaf and petiole deformations and other developmental abnormalities including enations. Enations have been related to infections of several viruses including ADV (Bejerman *et al.*, 2015), AEV-1 (Bejerman *et al.*, 2016), AMV (Trucco *et al.*, 2014) and southern rice black-streaked dwarf virus (SRBSDV; Xie *et al.*, 2014). Xie *et al.* (2014) reported that enations induced by the SRBSDV are highly organized and composed of new cytoplasmic bridges for trafficking virions across the interface between sieve elements of the phloem. The present study showed that the enations formed in the ribs during the ADV infection in alfalfa are determined by hyperplasia and hypertrophy of the fundamental parenchyma. In addition, contrary to that reported for other viruses such as SRBSDV (Xie *et al.*, 2014), vascularization was not observed in the enations. Interestingly, it was observed that epidermal cells have an average normal size and form, confirming the internal origin of the enations. This finding suggests that the irregular morphology of ribs and petioles of infected plants may be a result of an uncontrolled proliferation of cells from the fundamental parenchyma. In addition, when the leaf surfaces were analysed using SEM, a dense layer of epicuticular wax was observed on the surface of ADV-infected alfalfa. It has been suggested that the main function of the epicuticular wax is to work as a barrier against different pathogens, including viruses (Khan *et al*., 2011). Maxwell *et al.* (2016) speculated that there could be additional functions of the epicuticular wax induced by a virus infection. They proposed that

cucumber mosaic virus (CMV) could alter the leaf surface phenotype and epicuticular wax production in order to modify the polarization reflection properties and increase the attraction of the infected plant to aphids (Maxwell *et al.*, 2016).

Similar to the response against other biotrophic pathogens, plants infected by viruses deploy different defence methods, among them the production of H_2O_2 and deposition of callose (Iglesias & Meins, 2000; Xu *et al*., 2013). As observed in other long-term plant viral infections (Xu *et al*., 2013), alfalfa plants showed a long-term production of H_2O_2 during ADV infection. Interestingly, spots of H_2O_2 production were visualized along the midribs, suggesting that they could be areas of viral accumulation. Plants can also deploy additional mechanisms to avoid the systemic dissemination of virions, such as the induction of callose deposition and papillae formation (Iglesias & Meins, 2000). When the callose deposition was analysed in alfalfa leaflets infected with ADV, fluorescent localized spots were detected along the rib, similar to the H_2O_2 detection. In relation to these observations, some authors have reported that accumulation of H_2O_2 can be used by peroxidases to promote cross-linking of proteins and phenolic compounds to reinforce the cell wall in callose papillae (Thordal-Christensen *et al.*, 1997). Here, the colocalized increase in the long-term levels of H_2O_2 and callose deposition could be related to a cell wall reinforcement process induced by the viral infection (Xu *et al*., 2013). Other mechanisms of plant defence to biotic stress involve the induction of the systemic acquired response (SAR). This response is characterized by the induction of different pathogenesis-related genes such as *PR1*, *PR2*, *PR3*, *PR4* and *PR5* (van Loon *et al.*, 2006). When ADV-infected plants were analysed, a higher transcript expression of *PR5* was observed compared to control plants. This suggests that ADV may be involved in the elicitation of SAR in the host plant.

It is known that viruses alter the plant photosynthetic parameters during infection, affecting the normal plant growth and development (Pradhan *et al.*, 2015). Here, it was shown that ADV infection induces a drastic reduction in the net photosynthetic rate, stomatal conductance and the transpiration/evaporation rate of alfalfa plants. However, contrary to what was expected, high levels of Chl *a* and Chl *b* were observed in infected plants. Whereas in most plant–virus interactions the Chl *a*:Chl *b* ratio is affected (Bhattacharyya *et al*., 2015), in ADV-infected plants, no significant difference was observed in the Chl *a*:Chl *b* ratio compared to control plants. This suggests that the photosynthetic machinery from the infected plant is not damaged during the infection process. The balance in the Chl *a*:Chl *b* ratio is related to an efficient flux of electrons

through the photosystem I (PSI) and II (PSII) reaction centres. Liu *et al.* (2016) reported that dwarf rice (*Oryza sativa*) plants with BRs biosynthesis affected had significantly higher content of Chl *a* and Chl *b* but a similar Chl *a*:Chl *b* ratio. The authors suggested that BRs may have an effect on chlorophyll biosynthesis at the transcriptional level. To test this hypothesis, the transcript levels of the key genes involved in chlorophyll biosynthesis, *CHLH*, *CHLM* and *HEMC* (Liu *et al.*, 2016) were analysed. Higher expression levels of these genes were found during the infection of alfalfa by ADV, that would explain the high levels of chlorophylls and the darker green colour observed in infected plants. In order to find an explanation for these observations, the stomatal density and the number of opened and closed stomata were analysed. ADV-infected plants had a significantly lower number of stomata per mm^2 and a reduced proportion of open stomata compared to control plants. In this context, the stomatal density and aperture is highly regulated by different factors, including biotic stress (Murray *et al.*, 2016). Additionally, it has been shown that stomatal closure is an important factor limiting the uptake of CO_2 and the loss of water (Murray *et al.*, 2016). Moreover, Pradhan *et al*. (2015) reported that host plants infected with the wheat streak mosaic virus (WSMV) show a reduction in net photosynthesis as a result of stomatal closure. Taken together, these results suggest that the reduced photosynthetic rate in infected plants may be due to stomatal closure induced by ADV colonization.

Hormones play a key role in the regulation and maintenance of the plant response when affected by biotic or abiotic stresses. It is known that when viruses infect the host plant there are changes in physiological, biochemical and metabolic processes that involve the hormonal network (Paudel & Sanfaçon, 2018).

In order to investigate the role of the main phytohormones involved in regulating mechanisms related to morphological deformities and dwarfism (Shimada *et al.*, 2003; Sakamoto *et al.*, 2006; Cheng *et al.*, 2007; Argueso *et al.*, 2009), the transcript level of genes encoding proteins related to the biosynthesis of auxins, CKs and BRs were analysed. A significant reduction in expression of genes involved in the biosynthesis of BRs (*BR6OX2*), auxins (*YUC6*) and CKs (*IPT*) was observed in infected plants. In contrast, the gene *DWF4* had an increase in its expression in infected plants. Despite having a role in the biosynthesis of BRs, DWF4 has limited participation in the morphological changes attributed to this hormone (Sakamoto *et al.*, 2006), principally due to a feedback regulation mechanism of DWF4 modulated by the hormone level (Sakamoto *et al.*, 2006; Liu *et al.*, 2016).

Taken together, these results suggest a hormonal imbalance as a consequence of the ADV infection. The significant reduction in the expression levels of genes involved in the biosynthesis of auxins, CKs and BRs may be responsible for the physiological and morphological changes observed in the dwarfism of alfalfa plants during the viral infection.

The results here are consistent with the hypothesis that ADV induces different mechanisms of defence in the host plant. Additionally, an important alteration has been shown at the transcriptional level on chlorophyll biosynthesis that may be a mechanism to compensate for the drastic reduction in the photosynthetic rate. The results also suggest that this phenomenon could be due to drastic stomatal closure. Further studies are needed to understand the underlying mechanism involved in the development of the characteristic dwarfism phenotype during the viral infection. The findings, together with previous reports, will improve knowledge about viral interactions at the molecular level in alfalfa, which is a crop of global importance.

Acknowledgments

The authors thank Dr Adrián Vojnov, Abelardo Vegetti, Nora Uberti Manassero, Marcela Dotto and Jorgelina Ottado for scientific and technical assistance. They also thank Mauricio Minetti and José Maiztegui for the alfalfa plants used in this study. This work was supported by grants from the Agencia Santafesina de Ciencia, Tecnología e Innovación (ASaCTeI; project 2010-109-16) and from the Secretaría de Políticas Universitarias (SPU; project 9945) to G.D. G.D. and A.R. are staff members and S.M. is a Fellow of the Consejo Nacional de Investigaciones Científicas y Técnicas (CONICET, Argentina); G.J. is a staff member of the UNL; and C.J. is a Fellow of the SPU. The authors declare no conflict of interest.

References

Argueso CT, Ferreira FJ, Kieber JJ, 2009. Environmental perception avenues: the interaction of cytokinin and environmental response pathways. *Plant & Cell Environment* **32**, 1147–60.

Bejerman N, Nome C, Giolitti F *et al*., 2011. First report of a rhabdovirus infecting alfalfa in Argentina. *Plant Disease* **95**, 771.

Bejerman N, Giolitti F, De Breuil S *et al.*, 2015. Complete genome sequence and integrated protein localization and interaction map for alfalfa dwarf virus, which combines properties of both cytoplasmic and nuclear plant rhabdoviruses. *Virology* **483**, 275–83.

Bejerman N, Giolitti F, Trucco V, De Breuil S, Dietzgen RG, Lenardon S, 2016. Complete genome sequence of a new enamovirus from Argentina infecting alfalfa plants showing dwarfism symptoms. *Archive of Virology* **161**, 2029–32.

Bewick TA, Shilling DG, Querns R, 1993. Evaluation of epicuticular wax removal from whole leaves with chloroform. *Weed Technology* **7**, 706–16.

Bhattacharyya D, Gnanasekaran P, Kumar RK *et al*., 2015. A geminivirus betasatellite damages the structural and functional integrity of chloroplasts leading to symptom formation and inhibition of photosynthesis. *Journal of Experimental Botany* **66**, 5881–95.

Cheng Y, Dai X, Zhao Y, 2007. Auxin synthesized by the YUCCA flavin monooxygenases is essential for embryogenesis and leaf formation in *Arabidopsis*. *The Plant Cell* **19**, 2430–9.

Dunger G, Arabolaza AL, Gottig N, Orellano EG, Ottado J, 2005. Participation of *Xanthomonas axonopodis* pv. *citri hrp* cluster in citrus canker and nonhost plant responses. *Plant Pathology* **54**, 781–8.

Gonzalez AM, Marazzi B, 2018. Extrafloral nectaries in Fabaceae: filling gaps in structural and anatomical diversity in the family. *Botanical Journal of the Linnean Society* **187**, 26–45.

Gudesblat GE, Iusem ND, Morris PC, 2007. Guard cell-specific inhibition of *Arabidopsis MPK3* expression causes abnormal stomatal responses to abscisic acid and hydrogen peroxide. *New Phytologist* **173**, 713–21.

Hatsugai N, Hillmer R, Yamaoka S, Hara-Nishimura I, Katagiri F, 2016. The μ subunit of *Arabidopsis* adaptor protein-2 is involved in effector-triggered immunity mediated by membrane-localized resistance proteins. *Molecular Plant–Microbe Interactions* **29**, 35–51.

Iglesias VA, Meins F, 2000. Movement of plant viruses is delayed in a β-1,3-glucanase-deficient mutant showing a reduced plasmodesmatal size exclusion limit and enhanced callose deposition. *The Plant Journal* **21**, 157–66.

Jin L, Qin Q, Wang Y *et al.*, 2016. Rice dwarf virus P2 protein hijacks auxin signaling by directly targeting the rice OsIAA10 protein, enhancing viral infection and disease development. *PLoS Pathogens* **12**, e1005847.

Khan MAU, Shahid AA, Rao AQ *et al.*, 2011. Role of epicuticular waxes in the susceptibility of cotton leaf curl virus (CLCuV). *African Journal of Biotechnology* 10, 17868–74.

Lenardon S, Pérez Fernández J, Basigalup D, 2010. Descubren una nueva enfermedad en alfalfa. INTA Informa. Buenos Aires, Argentina: INTA. [http://intainforma.inta.gov.ar/?p=2693]. Accessed 30 August 2019.

Liu X, Feng ZM, Zhou CL *et al.*, 2016. Brassinosteroid (BR) biosynthetic gene *lhdd10* controls late heading and plant height in rice (*Oryza sativa* L.). *Plant Cell Reporter* **35**, 357–68.

Livak KJ, Schmittgen TD, 2001. Analysis of relative gene expression data using real-time quantitative PCR and the $2^{-\Delta\Delta Ct}$ method. *Methods* **25**, 402–8.

van Loon LC, Rep M, Pieterse CMJ, 2006. Significance of inducible defense-related proteins in infected plants. *Annual Review of Phytopathology* **44**, 135–62.

Mann KS, Bejerman N, Johnson KN, Dietzgen RG, 2016. *Cytorhabdovirus* P3 genes encode 30K-like cell-to-cell movement proteins. *Virology* **489**, 20–33.

Maxwell DJ, Partridge JC, Roberts NW, Boonham N, Foster GD, 2016. The effects of plant virus infection on polarization reflection from leaves. *PLoS ONE* **11**, e0152836.

Murray RR, Emblow MSM, Hetherington AM, Foster GD, 2016. Plant virus infections control stomatal development. *Science Reporter* **6**, 34507.

Paudel DB, Sanfaçon H, 2018. Exploring the diversity of mechanisms associated with plant tolerance to virus infection. *Frontiers in Plant Science* **9**, 1575.

Pradhan GP, Xue Q, Jessup KE, Hao B, Price JA, Rush CM, 2015. Physiological responses of hard red winter wheat to infection by *Wheat streak mosaic virus*. *Phytopathology* **105**, 621–7.

Radović J, Sokolović D, Marković J, 2009. Alfalfa – most important perennial forage legume in animal. *Biotechnology in Animal Husbandry* **25**, 465–75.

Sakamoto T, Morinaka Y, Ohnishi T *et al.*, 2006. Erect leaves caused by brassinosteroid deficiency increase biomass production and grain yield in rice. *Nature Biotechnology* **24**, 105–9.

Samac DA, Rhodes LH, Lamp WO, 2014. *Compendium of Alfalfa Diseases and Pests*. 3rd edn. St Paul, MN, USA: APS Press.

Samarfard S, Bejerman NE, Dietzgen RG, 2018. Distribution and genetic variability of alfalfa dwarf virus, a cytorhabdovirus associated with alfalfa dwarf disease in Argentina. *Virus Genes* **54**, 612–5.

Shimada Y, Goda H, Nakamura A, Takatsuto S, Fujioka S, Yoshida S, 2003. Organ-specific expression of brassinosteroid-biosynthetic genes and distribution of endogenous brassinosteroids in *Arabidopsis*. *Plant Physiology* **131**, 287–97.

Thordal-Christensen H, Zhang Z, Wei Y, Collinge DB, 1997. Subcellular localization of H_2O_2 in plants. H_2O_2 accumulation in papillae and hypersensitive response during the barley–powdery mildew interaction. *The Plant Journal* **11**, 1187–94.

Trucco V, De Breuil S, Bejerman N, Lenardon S, Giolitti F, 2014. Complete nucleotide sequence of *Alfalfa mosaic virus* isolated from alfalfa (*Medicago sativa* L.) in Argentina. *Virus Genes* **48**, 562–5.

Wellburn AR, 1994. The spectral determination of chlorophylls *a* and *b*, as well as total carotenoids, using various solvents with spectrophotometers of different resolution. *Journal of Plant Physiology* **144**, 307–13.

Whitfield AE, Huot OB, Martin KM, Kondo H, Dietzgen RG, 2018. Plant rhabdoviruses-their origins and vector interactions. *Current Opinion in Virology* **33**, 198–207.

Xie L, Lv MF, Zhang HM, Yang J, Li JM, Chen JP, 2014. Tumours induced by a plant virus are derived from vascular tissue and have multiple intercellular gateways that facilitate virus movement. *Journal of Experimental Botany* **65**, 4873–86.

Xu Q, Ni H, Chen Q *et al*., 2013. Comparative proteomic analysis reveals the cross-talk between the responses induced by H_2O_2 and by long-term rice black-streaked dwarf virus infection in rice. *PLoS ONE* **8**, e81640.

Zavaliev R, Epel BL, 2015. Imaging callose at plasmodesmata using aniline blue: quantitative confocal microscopy. *Methods in Molecular Biology* **1217**, 105–19.

Supporting Information

Additional Supporting Information may be found in the online version of this article at the publisher's web-site.

Figure S1 Scanning electron microscopy of alfalfa leaves. Abaxial (a and b), and adaxial (c) side of alfalfa leaves. Control and ADV indicate mock inoculated and alfalfa dwarf virus-infected plants, respectively. Size bars = 100 μm.

Table S1 Primers used in this study. Primer pairs were designed using PRIMER3PLUS software (https://primer3plus.com/). (a) Accession number from the National Center for Biotechnology Information (NCBI; https://www.ncbi.nlm.nih.gov); (b) contig number from the Alfalfa Gene Index and Expression Atlas Database (AGED; http://plantgrn.noble.org/AGED/index.jsp).

Figure legends

Figure 1 Alfalfa dwarf virus (ADV) affects the morphology of alfalfa plants. (a) Comparative phenotypes of alfalfa plants mock-inoculated with buffer (control) or inoculated with ADV. Enations were observed in midribs (b, c) and petioles (d) of infected leaves. (c) corresponds to a magnification of the box shown in (b).

Figure 2 Epidermal cells are not affected during the development of the enations. Scanning electron microscopy of abaxial side of alfalfa leaves. Plants were either mock-inoculated with buffer (control) or inoculated with alfalfa dwarf virus (ADV).

Figure 3 Enations are caused by a disorganization of the fundamental parenchyma. Histological analysis of leaflets mock-inoculated with buffer (control) or with alfalfa dwarf virus (ADV), and stained with safranin and astra blue. (a) Secondary vascular bundles; (b) main vascular bundles; (c) magnification of the central region of the main vascular bundles. The black arrows indicate the fundamental parenchyma.

Figure 4 Alfalfa dwarf virus (ADV) induces biochemical alteration in alfalfa plants. (a) Hydrogen peroxide production observed by reaction with DAB. (b) Magnification of the white box shown in (a). (c) Callose deposition stained with aniline blue and observed by fluorescent microscopy. (d) Magnification of the box shown in (c). (e) DAB staining intensity calculated based on the pixel intensity of five photographs per treatment using IMAGEJ. (f) Number of callose deposits observed in an area of 1 mm^2 and calculated using IMAGEJ. (g) Transcript expression level of the pathogenesis-related gene *PR5* in infected plants relative to the control as determined by qRT-PCR. Plants were mock-inoculated with buffer (control) or with ADV. Each bar represents the mean ± standard errors (SE) of three independent experiments. Asterisks indicate statistically significant differences between treatments (* $P < 0.05$ or *** $P < 0.001$) by Student's *t*-test.

Figure 5 Alfalfa dwarf virus (ADV) induces the accumulation of epicuticular wax. SEM of abaxial side of leaves mock-inoculated with buffer (control) or with ADV (a, b). (c) Total content of wax. Each bar represents the mean ± standard errors (SE) of three independent experiments. Asterisks indicate statistically significant differences between treatments (*** $P < 0.001$) by Student's *t*-test.

Figure 6 Alfalfa dwarf virus affects the photosynthetic parameters. (a) Net photosynthesis rate (Pn); (b) stomatal conductance rate (Gs); and (c) transpiration/evaporation rate (E) measured on leaves mock-inoculated with buffer (control) or with alfalfa dwarf virus (ADV) using a CIRAS-2 system. Experiments were performed maintaining constant CO_2 concentration (500 ppm) and photon flux density (900 μmol m^{-2} s^{-1}). Each bar represents the mean ± standard errors (SE) of three independent experiments. Asterisks indicate statistically significant differences between treatments (** $P < 0.01$ or *** $P < 0.001$) by Student's *t*-test.

Figure 7 Alfalfa dwarf virus infection induces a hormonal imbalance and alters the number of stomata. (a) Number of opened/closed stomata per mm^2. (b) Transcriptional analysis of the

chlorophyll biosynthesis genes *hydroxymethylbilane synthase* (*HEMC*), *magnesium-chelatase subunit chlH* (*CHLH*) and *magnesium-protoporphyrin IX methyltransferase* (*CHLM*), and (c) the hormonal biosynthesis genes *brassinosteroid-6-oxidase 2* (*BR6OX2*), *steroid 22-alpha-hydroxylase* (*DWF4*), *YUCCA flavin monooxygenase 6* (*YUC6*) and *isopentenyl transferase* (*IPT*) observed by qRT-PCR. Each bar represents the mean ± standard errors (SE) of three independent experiments. Asterisks indicate statistically significant differences between treatments (* $P < 0.05$ or ** $P < 0.01$) by Student's *t*-test.

Table 1. Chlorophyll pigments quantification.

	Chl a[a] (mg g^{-1} FW)	**Chl b[b] (mg g^{-1} FW)**	**Chl a/Chl b**
Control	62.010±2.544	22.709±1.873	2.761±0.475
ADV	92.526±1.286^{**1}	36.399±1.641^{*2}	2.541±0.251^{nsd}

Spectrophotometric quantification of photosynthetic pigments from leaves inoculated with mock buffer (control) or with alfalfa dwarf virus (ADV). a corresponds to chlorophyll a; b indicates chlorophyll b. FW, Fresh weight. Each value represents the mean ± standard errors (SE) of three independent experiments. Asterisks indicate statistically significant differences between control and ADV infected plants, **1, p=0.0022 ($p < 0.01$, n=5); *2, p=0.014 ($p < 0.05$, n=5); nsd, not significant difference.

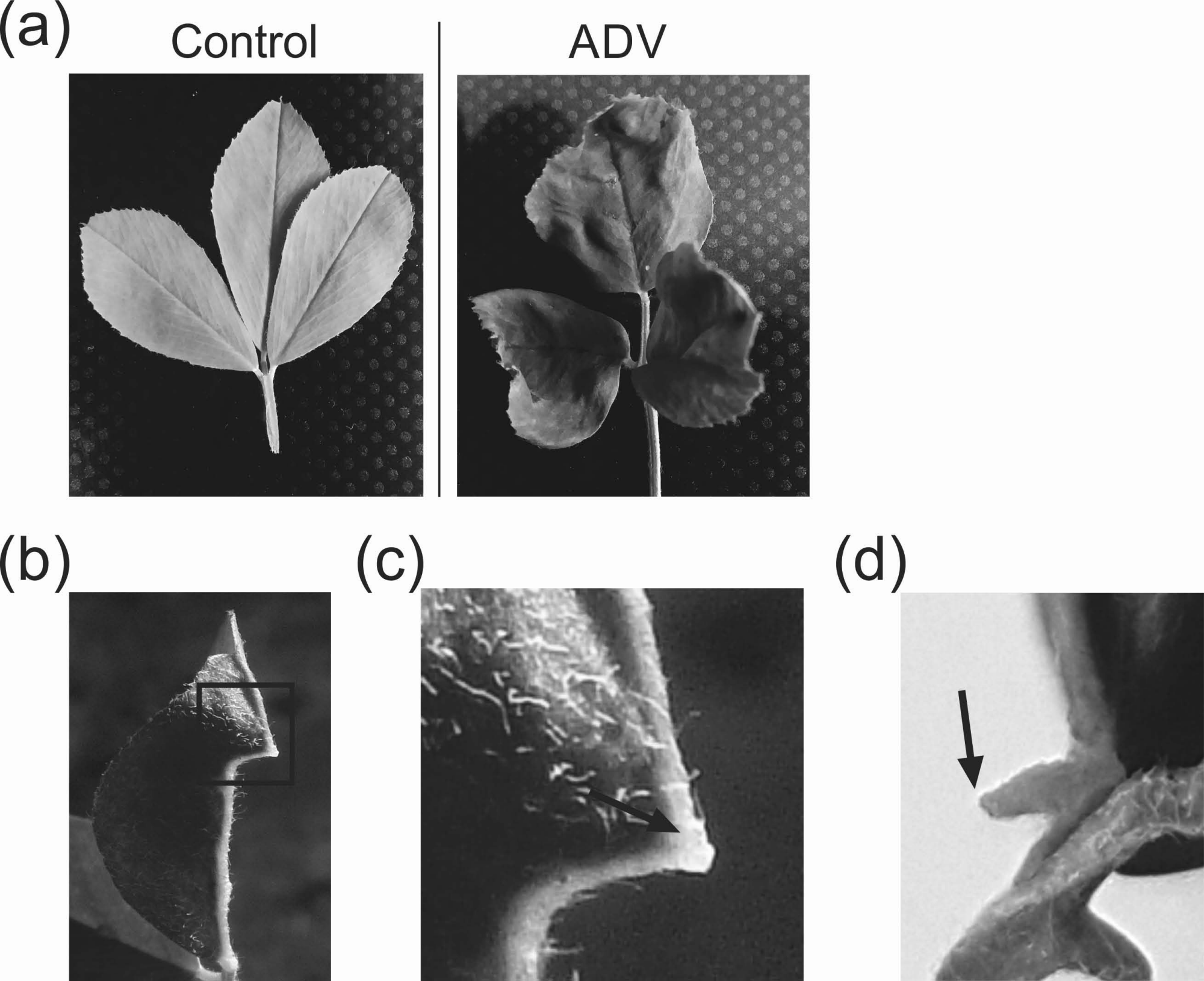
(a)
Control
ADV
(b)
(c)
(d)

Control

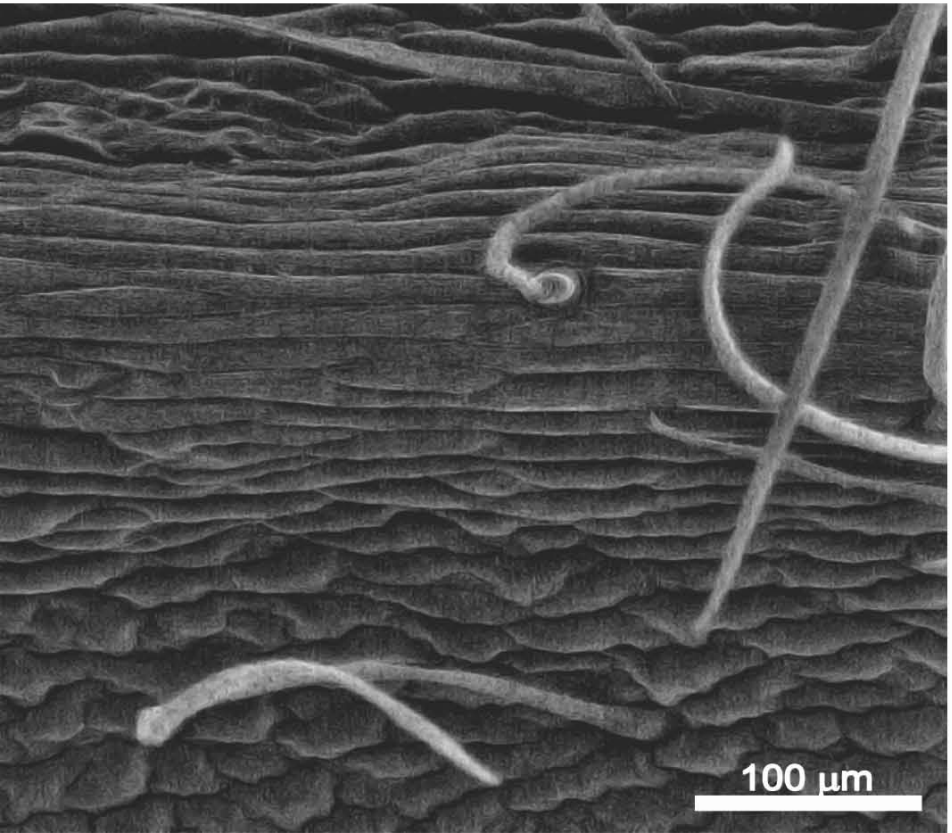

ADV

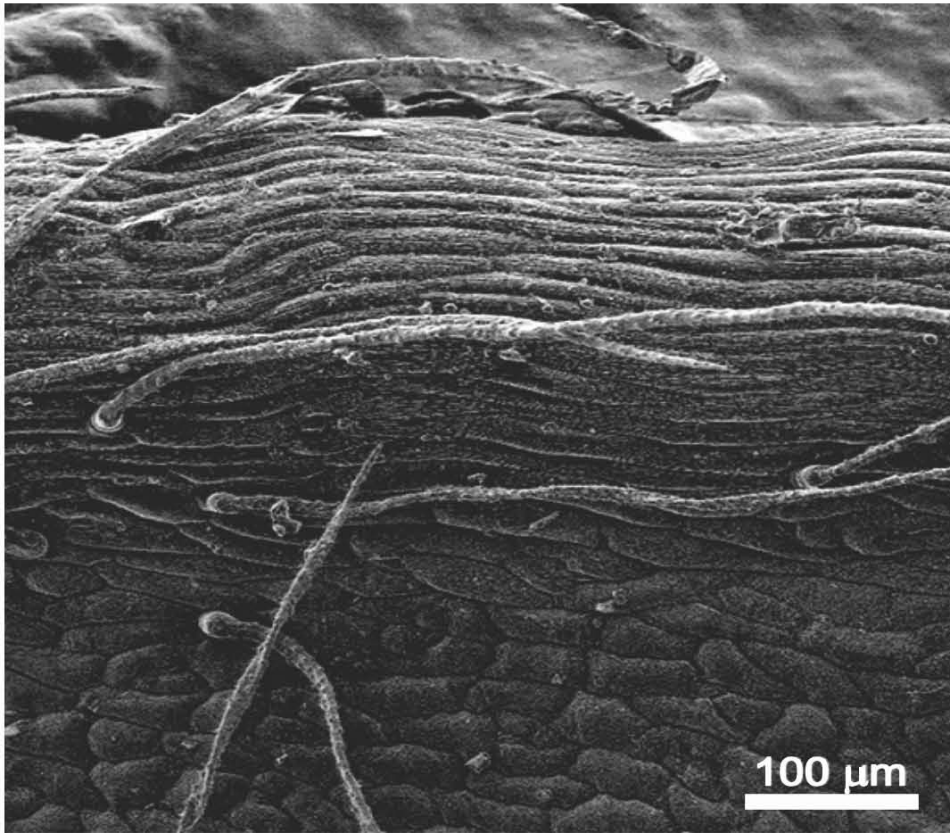

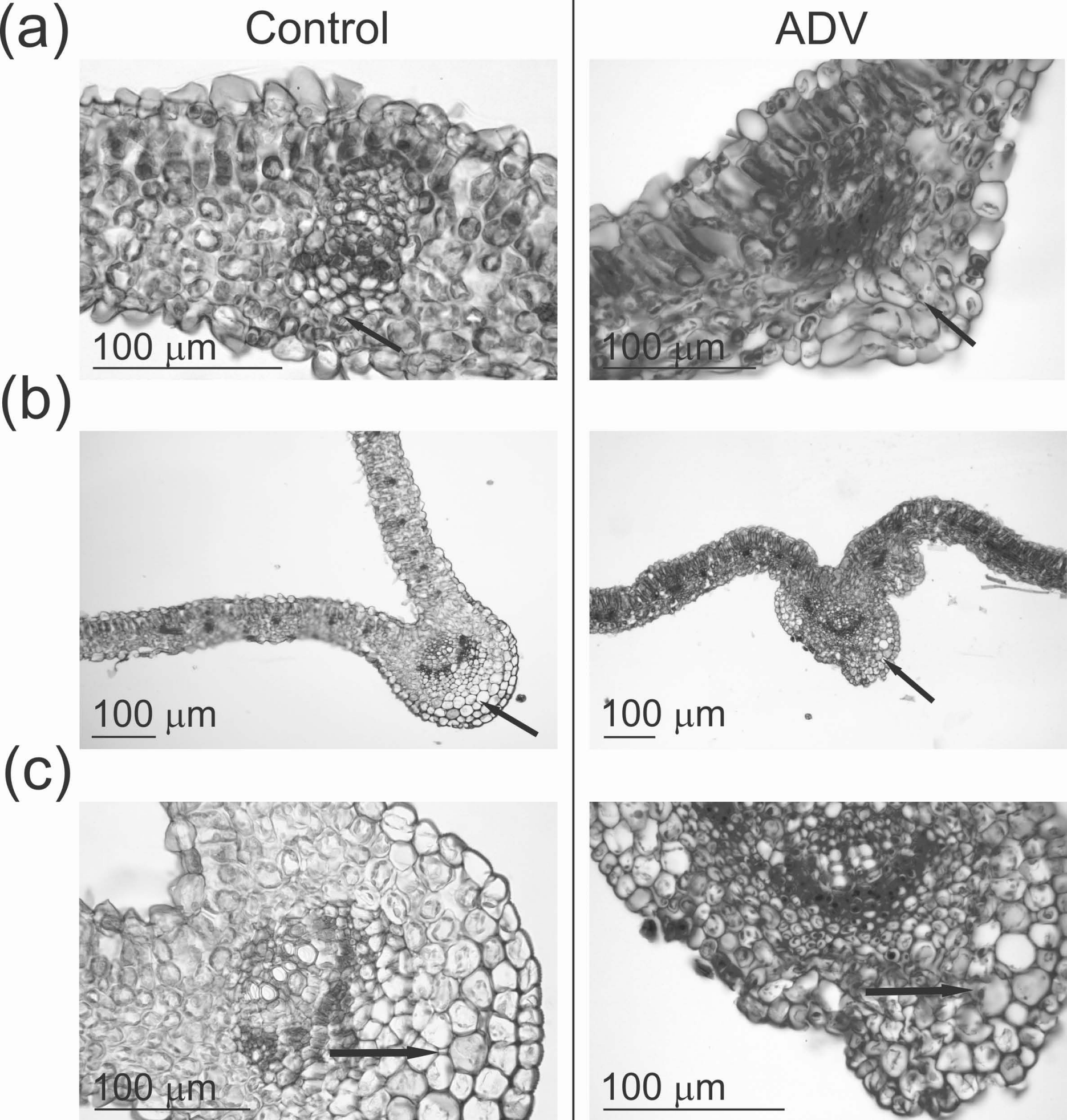
(a)
Control
ADV
100 μm
100 μm
(b)
100 μm
100 μm
(c)
100 μm
100 μm

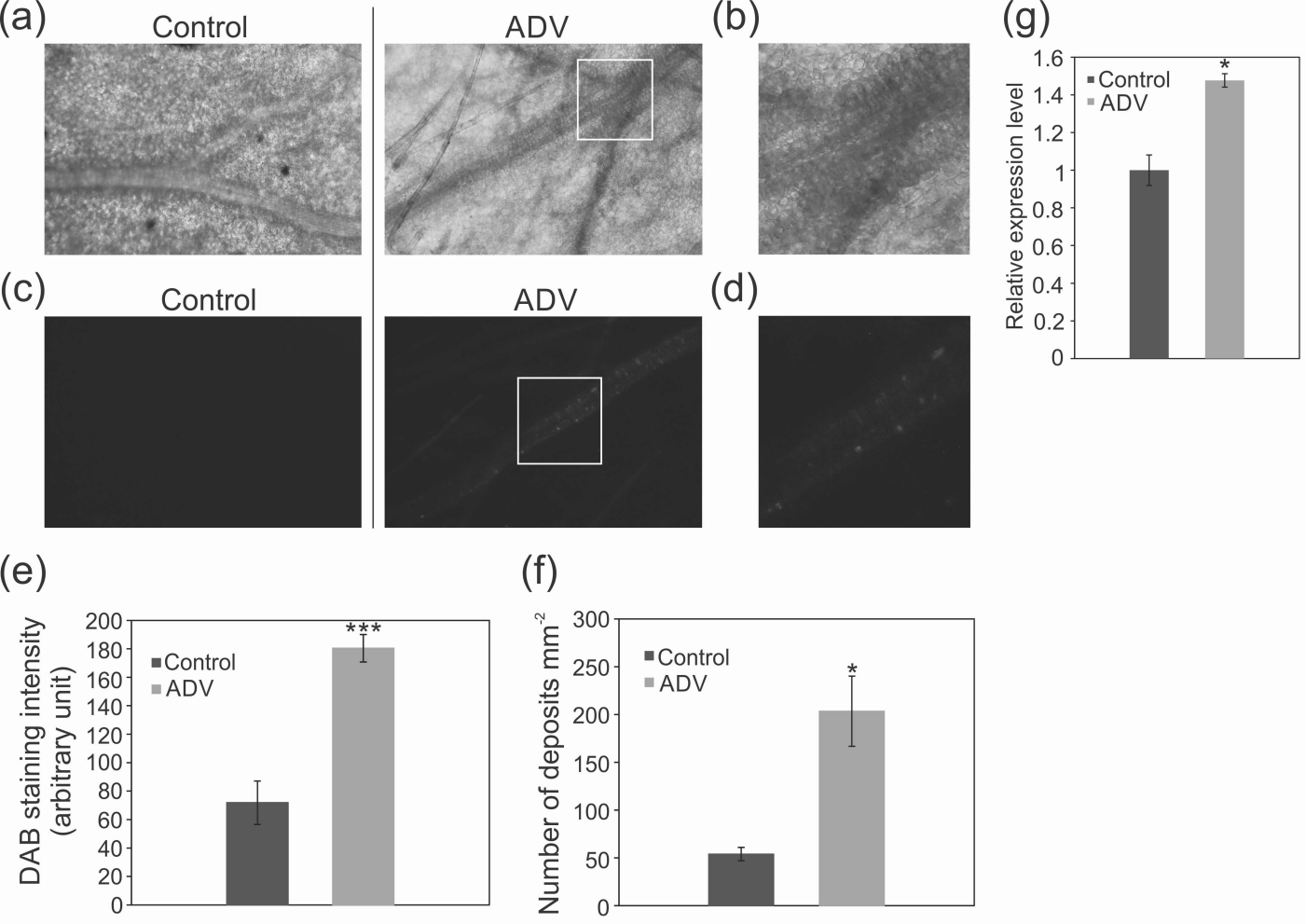
(a)
Control
ADV
(b)
(c)
Control
ADV
(d)
(g)
Relative expression level
Control
ADV
*
(e)
DAB staining intensity (arbitrary unit)
Control
ADV
***
(f)
Number of deposits mm-2
Control
ADV
*

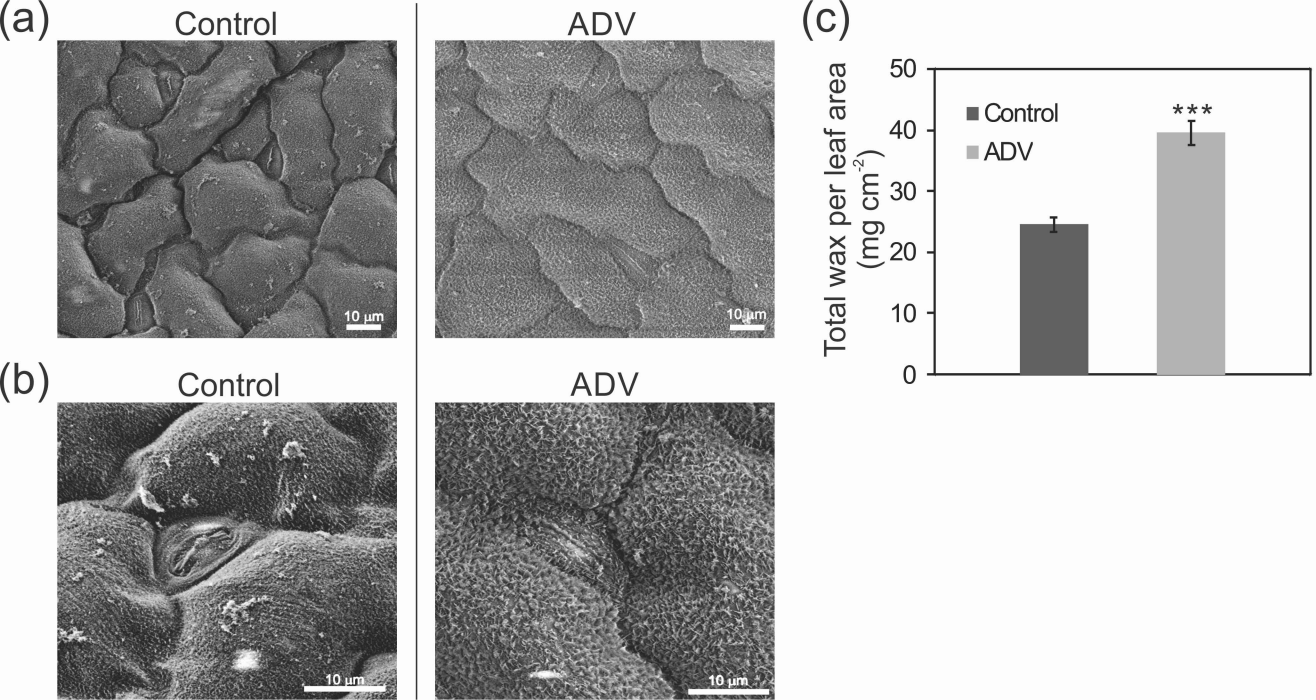
(a)
Control
ADV
10 µm
10 µm
(b)
Control
ADV
10 µm
10 µm
(c)
Total wax per leaf area (mg cm-2)
50
40
30
20
10
0
Control
ADV
***

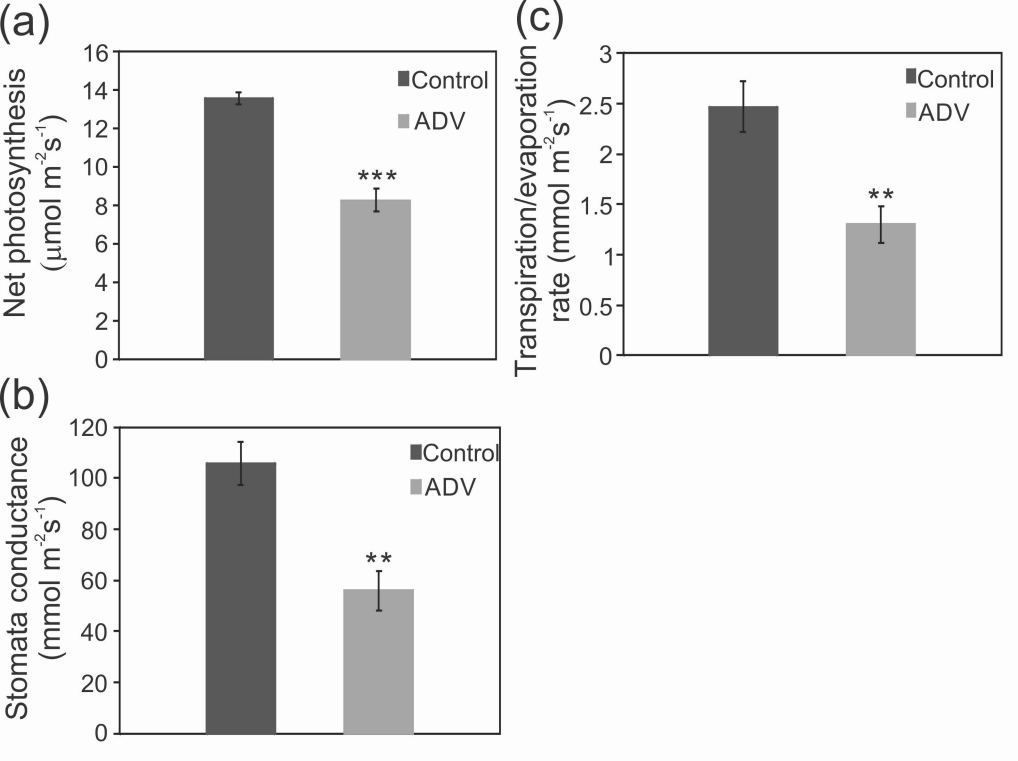
(a)
Net photosynthesis (μmol m-2s-1)
16
14
12
10
8
6
4
2
0
Control
ADV
***
(c)
Transpiration/evaporation rate (mmol m-2s-1)
3
2.5
2
1.5
1
0.5
0
Control
ADV
**
(b)
Stomata conductance (mmol m-2s-1)
120
100
80
60
40
20
0
Control
ADV
**

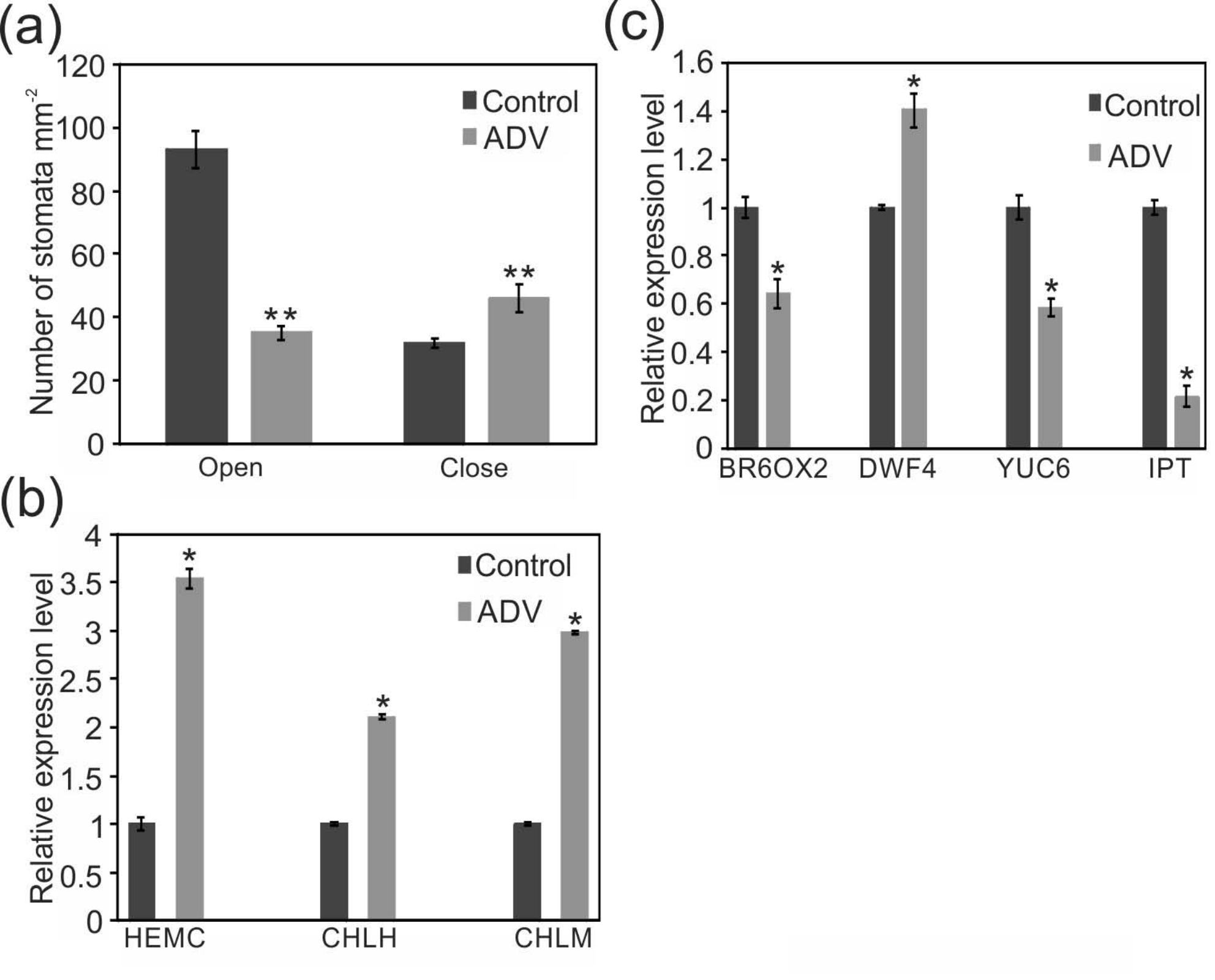
(a)
Number of stomata mm-2
120
100
80
60
40
20
0
Control
ADV
**
**
Open
Close
(b)
Relative expression level
4
3.5
3
2.5
2
1.5
1
0.5
0
Control
ADV
*
*
*
HEMC
CHLH
CHLM
(c)
Relative expression level
1.6
1.4
1.2
1
0.8
0.6
0.4
0.2
0
Control
ADV
*
*
*
*
BR6OX2
DWF4
YUC6
IPT